Article

Numerical Study on Ammonia Dispersion and Explosion Characteristics in Confined Space of Marine Fuel Preparation Room

Phan Anh Duong [1,†], Jin-Woo Bae [2,†], Changmin Lee [1], Dong Hak Yang [3] and Hokeun Kang [4,*]

1   Maritime Industry Research Institute, National Korea Maritime and Ocean University, 727, Taejong-ro, Yeongdo-gu, Busan 49112, Republic of Korea; anhdp@g.kmou.ac.kr (P.A.D.); oldbay@kmou.ac.kr (C.L.)
2   Division of Ocean Polytech, Korea Institute of Maritime and Fisheries Technology, Busan 49111, Republic of Korea; qowlsdn3@seaman.or.kr
3   Mechanical Convergence Industry Standards Division, Korean Agency for Technology and Standards, 93, Isu-ro, Eumseong-gun, Maengdong-myeon 27737, Chungcheongbuk-do, Republic of Korea; danghak@korea.kr
4   Division of Marine Systems Engineering, National Korea Maritime and Ocean University, 727, Taejong-ro, Yeongdo-gu, Busan 49112, Republic of Korea
*   Correspondence: hkkang@kmou.ac.kr; Tel.: +82-51-410-4260; Fax: +82-51-404-3985
†   These authors contributed equally to this work.

Abstract

Ammonia is emerging as a promising zero-carbon marine fuel due to its high hydrogen density, low storage pressure, and long-term stability, making it well-suited for supporting sustainable maritime energy systems. However, its adoption introduces serious safety challenges, as its toxic, flammable, and corrosive properties pose greater risks than many other alternative fuels, necessitating rigorous risk assessment and safety management. This study presents a comprehensive investigation of potential ammonia leakage scenarios that may arise during the fuel gas supply process within confined compartments of marine vessels, such as the fuel preparation room and engine room. The simulations were conducted using FLACS-CFD V22.2, a validated computational fluid dynamics tool specialized for flammable gas dispersion and explosion risk analysis in complex geometries. The model enables detailed assessment of gas concentration evolution, toxic exposure zones, and overpressure development under various leakage conditions, providing valuable insights for emergency planning, ventilation design, and structural safety reinforcement in ammonia-fueled ship systems. Prolonged ammonia exposure is driven by three key factors: leakage occurring opposite the main ventilation flow, equipment layout obstructing airflow and causing gas accumulation, and delayed sensor response due to recirculating flow patterns. Simulation results revealed that within 1.675 s of ammonia leakage and ignition, critical impact zones capable of causing fatal injuries or severe structural damage were largely contained within a 10 m radius of the explosion source. However, lower overpressure zones extended much further, with slight damage reaching up to 14.51 m and minor injury risks encompassing the entire fuel preparation room, highlighting a wider threat to crew safety beyond the immediate blast zone. Overall, the study highlights the importance of targeted emergency planning and structural reinforcement to mitigate explosion risks in ammonia-fueled environments.

Keywords: ammonia; FGSS; marine vessels; risk assessment; consequence analysis; dispersion

1. Introduction

Maritime transportation serves as a cornerstone of the global economy, facilitating over 80% of international trade by volume. Owing to its substantial cargo capacity, high operational safety, and cost-effectiveness, it remains a preferred mode for long-distance freight movement. However, the continued growth of global shipping activities is projected to result in a substantial increase in greenhouse gas (GHG) emissions, positioning the maritime sector as an increasingly prominent contributor to anthropogenic climate change [1–3]. In response to the urgent need to mitigate its environmental impact, the maritime shipping industry is actively pursuing strategies to substantially reduce greenhouse gas (GHG) emissions. The International Maritime Organization (IMO) has set ambitious targets, including net-zero GHG emissions by 2050, a 40% decrease in carbon dioxide (CO_2) emissions per transport work by 2030, relative to 2008 levels [4–6]. To enhance energy efficiency in shipping and reduce carbon dioxide (CO_2) emissions, the International Maritime Organization (IMO) has enacted several regulatory measures under MARPOL Annex VI. Key initiatives include the Ship Energy Efficiency Management Plan (SEEMP), the Energy Efficiency Design Index (EEDI), and the Energy Efficiency Operational Indicator (EEOI), all of which came into effect on 1 January 2013 [7,8]. Identifying alternative fuel sources is critical to meeting the growing energy demands of marine transportation while achieving decarbonization goals [9,10].

Hydrogen has emerged as a promising zero-carbon energy carrier, offering a high specific energy by mass. It can be utilized across a range of propulsion technologies including internal combustion engines (ICEs), fuel cells [11,12], and gas turbines, making it a versatile candidate for supporting the maritime sector's transition toward low-emission operations [13–15]. Despite its environmental advantages, hydrogen's low volumetric energy density poses significant challenges for marine applications, as it necessitates substantial onboard storage volume and can limit voyage duration. These limitations adversely affect the economic viability and operational efficiency of vessels. Consequently, there is a pressing need to explore alternative hydrogen carrier fuels that can fulfill both emission reduction objectives and the practical requirements of ship operation and logistics management [16]. Ammonia has gained significant attention as a promising alternative marine fuel, primarily due to its carbon-free composition, which aligns well with IMO decarbonization targets. In addition to its potential as a fuel, ammonia is also being explored as an efficient hydrogen carrier, as it enables hydrogen to be stored in liquid form at ambient temperature and offers a higher volumetric hydrogen density compared to liquefied hydrogen [5,6,17].

Ammonia possesses a high-octane rating ranging from 110 to 130 and a narrow flammability range, which contributes to its relatively low explosion risk and enhances its safety profile for marine applications. Additionally, its favorable power-to-fuel-to-power (PFP) efficiency and the existence of a well-established global distribution infrastructure further support its viability as an alternative marine fuel [18]. The growing adoption of ammonia as a marine fuel has led to a corresponding rise in the demand for ammonia bunkering infrastructure and services [19,20]. Unlike the conventional liquid fuel gas supply system (FGSS), ammonia FGSS presents unique hazards due to the handling of cryogenic or high-pressure liquid transfer and vapor return systems. These factors necessitate stringent safety protocols, as any accidental release of ammonia during bunkering operations could pose severe safety and environmental risks [21,22]. Such incidents may occur through a sequence of failures, where one or more safety systems designed to prevent ammonia leakage malfunction are bypassed, ultimately resulting in the uncontrolled release and dispersion of ammonia into the surrounding environment [22,23]. Ignition of the released ammonia vapor may trigger fires or explosions [9], potentially disrupting standard ammonia FGSS

operations. To quantify the probability and consequences of such ammonia releases, risk assessment models are employed, providing critical insights for safety management and mitigation planning [24,25]. Therefore, ensuring safety in ammonia FGSS operations is of paramount importance and must be thoroughly addressed [26–28].

While ammonia offers promising environmental and operational benefits as a marine fuel, its widespread adoption necessitates a deeper understanding of the associated safety risks particularly concerning its leakage, dispersion, and explosion behavior in complex operational environments. Zhang et al. [29] conducted research on the leakage and diffusion behavior of ammonia, with a primary focus on liquid ammonia and its relevance to practical engineering scenarios. However, comprehensive safety studies on ammonia are still in their early developmental stages. Existing investigations into ammonia's combustion and explosion properties have largely concentrated on flame dynamics and combustion behavior. Notably, ammonia is recognized as an effective medium for hydrogen storage, where the interconversion between hydrogen and ammonia can occur simultaneously across both spatial and temporal domains. Despite this potential, current research has yet to adequately explore the safety risks associated with the handling and utilization of hydrogen–ammonia mixtures during application processes. Li et al. [30] conducted an experimental investigation into the explosion characteristics of hydrogen–ammonia–air mixtures, focusing on flame behavior and explosion pressure under varying equivalence ratios (ER) and ammonia fractions (AF). The study revealed that both the average flame propagation velocity (AFPV) and maximum explosion pressure (MEP) decreased progressively with higher ammonia content. In contrast, as the equivalence ratio increased, these parameters initially rose and then declined. Specifically, the peak values of AFPV and MEP were observed at ER = 1.4 for AF = 0.1, ER = 1.2 for AF = 0.3, and ER = 1.0 for both AF = 0.5 and AF = 0.7. The results also indicated that conventional laminar and turbulent flame models may, respectively, underestimate or overestimate MEP values, particularly when flame instabilities are neglected. Furthermore, an increase in ammonia fraction led to reductions in adiabatic flame temperature and thermal diffusivity, which in turn contributed to a decline in laminar burning velocity (LBV), significantly influencing the explosion pressure. Li et al. [31] examined the influence of ammonia concentration on explosion pressure, flame propagation behavior, and the underlying microscopic reaction mechanisms. Their findings showed that both the maximum explosion pressure and the peak pressure rise rate initially increased with ammonia concentration, peaking at 0.23 MPa and 8.7 MPa·s^{-1}, respectively, at a concentration of 22 vol%, before declining at higher concentrations. The trends observed in flame propagation mirrored those of the pressure response. In combustion simulations, a positive correlation was identified between system density and both reaction rates and energy conversion efficiency. Additionally, as system density increased, the time required for key reactive intermediates such as NH_2, OH, and NHO to reach their peak concentrations decreased, indicating a faster progression of the combustion chain reactions. Bae et al. [32] conducted a detailed investigation into how the location of the ignition source affects ammonia explosion behavior within a fuel preparation room. Using computational fluid dynamics (CFD) simulations implemented in the FLACS platform, the study analyzed critical explosion parameters, including peak overpressure, pressure rise rate, flammable gas depletion, ignition delay time, and the spatial–temporal evolution of temperature and combustion byproducts. The findings highlight that the ignition source location significantly influences the explosion dynamics. Specifically, ignition near the ceiling produced the most severe outcome, with a maximum overpressure of 4.27 bar and a rapid pressure rise rate of 2.20 bar/s, indicating a highly hazardous scenario. Conversely, ignition along the forward wall resulted in the lowest peak overpressure (3.24 bar) and minimal flame propagation, representing a comparatively

less dangerous condition. Tan et al. [33] investigated the dispersion behavior of ammonia within a food processing facility, highlighting that the dispersion characteristics are governed by the compound's physical properties, the conditions at the release source, and the surrounding atmospheric environment. Due to its lower density compared to air, ammonia exhibited upward movement near the release point and tended to concentrate along the central axis. The study found that wind conditions significantly influenced the dispersion pattern, with the most pronounced effects occurring at wind speeds between 0.8 and 1.2 m/s. Variations in both the height of the release source and the measurement points had a substantial impact on observed concentration levels. The dispersion behavior of ammonia also analyzed with CFD method by various researchers such as [34–36]. Among the computational models assessed, the RNG k-ε turbulence model demonstrated the best agreement with experimental data. The simulation results revealed that ammonia dispersion is characterized by steep concentration gradients and that horizontal wind flow effectively steers its movement.

In summary, existing research on the diffusion and explosion characteristics of ammonia leaks within ship fuel preparation rooms remains limited, with few studies addressing the combined influence of multiple interacting factors on gas behavior. Unlike conventional confined spaces, marine fuel preparation rooms present a distinct and complex environment shaped by structural design, equipment configuration, ventilation dynamics, and heat transfer processes. Moreover, the maritime context introduces additional challenges compared to onshore facilities, including harsher operational conditions, elevated safety risks, and greater difficulty in emergency response. These unique characteristics underscore the need for targeted investigations tailored to the realities of marine operations.

To address this gap, the present study developed a three-dimensional model of a marine fuel preparation room to analyze ammonia diffusion under the influence of various coupled parameters. Based on the simulation outcomes, vapor cloud explosion (VCE) scenarios were constructed to evaluate potential hazards. Recognizing the absence of established guidelines for determining explosion intensity levels in prior research, this study conducted a comparative analysis between the TNO Multi-Energy (ME) method and Computational Fluid Dynamics (CFD) simulations. This comparison provides a reference framework for selecting appropriate explosion strength levels. Additionally, safety distances were estimated based on the projected damage extent. The results contribute valuable theoretical insights for improving accident prevention and emergency response strategies in ship engine rooms, helping to bridge the knowledge gap in the current literature.

2. Characteristics of Ammonia

2.1. Overview and Physicochemical Characteristics of Ammonia

Ammonia (NH_3) is a compound consisting of one nitrogen atom bonded to three hydrogen atoms. It is a colorless gas characterized by a sharp, penetrating odor. With a hydrogen content of approximately 17.6% by weight, ammonia possesses a lower heating value of about 22.5 MJ/kg, making it a potential candidate for use as an alternative fuel [37–39]. The average market price of ammonia typically ranges between $250 and $300 per metric ton [40]. Globally, the ammonia production process is responsible for approximately 1% of total greenhouse gas (GHG) emissions, highlighting its significant environmental impact despite its widespread industrial use [41]. Ammonia possesses several favorable characteristics that make it a promising candidate for use as both a fuel and a hydrogen carrier. Notably, its volumetric hydrogen density is approximately 45% higher than that of liquid hydrogen, indicating that liquid ammonia can store a greater amount of hydrogen within the same volume. This enhanced storage capacity underscores its potential in hydrogen transport and energy applications [42]. Among common hydrogen

carriers such as ethanol, methanol, liquid hydrogen, and gasoline, ammonia stands out for its superior volumetric hydrogen density, allowing it to store more hydrogen per unit volume than these conventional fuels [43]. Compared to hydrogen, another carbon-free energy carrier, ammonia offers a more practical and less demanding storage solution. It can be stored either at ambient temperature under a pressure of approximately 10 bar or at a moderate temperature of 33 °C under atmospheric pressure, simplifying handling and infrastructure requirements [38]. Table 1 summarizes the fundamental physical and chemical properties of ammonia.

Table 1. An overview of ammonia's key characteristics [44].

Properties	Unit	Value
Energy content per unit mass	MJ/L	12.7
Latent heat required for phase change (Vaporization)	MJ/kg	188
Auto-Ignition temperature	°C	651
Standard density (at 0 °C and 1 atm)	kg/m^3	0.769
Specific heat capacity at constant pressure (Cp)	kJ/mol °C	0.037
Equilibrium vapor pressure at 20 °C	kPa	858
Specific heat capacity at constant volume (Cv)	kJ/mol °C	0.028
Enthalpy of vaporization	kJ/kg	1371
Adiabatic flame temperature at 1 atm	°C	1800
Vapor pressure required for condensation at 25 °C	MPa	0.99
Minimum energy required for ignition	mJ	680
Flammability limits in dry air	%	15.15 to 27.35
Liquid phase density	kg/m^3	600
Cetane rating		0
Molecular weight	g/mol	17.031
Maximum adiabatic flame temperature	°C	1800
Freezing point	°C	−77.7
Octane rating		~130
Boiling temperature at atmospheric pressure (1 atm)	°C	−33.6
Critical temperature	°C	132.25
Maximum laminar flame speed	m/s	0.07
Critical pressure	bar	113

Due to its toxic and corrosive properties, ammonia requires stringent safety measures during storage. Its hazard potential is significantly greater exceeding that of commonly used fuels like methanol and diesel by more than threefold necessitating enhanced precautions to ensure safe handling [45]. If ammonia is released into aquatic environments, it can pose toxicity risks to marine organisms. However, natural processes such as biodegradation and the nitrogen cycle can help restore the affected ecosystems over time. Additionally, ammonia is detectable at extremely low concentrations due to its very low odor threshold ranging from 0.037 to 1.0 ppm, allowing most people to perceive its presence even at levels below those harmful to human health.

Gaseous ammonia is less dense than air, with a density of approximately 0.769 kg/m^3 compared to air's 1.225 kg/m^3 at standard temperature and pressure (STP). This lower density allows ammonia to disperse rapidly into the atmosphere under normal environmental conditions, thereby reducing the likelihood of fire or explosion following a leak. Furthermore, ammonia has a higher auto-ignition temperature of around 650 °C, which is notably greater than hydrogen's 520 °C, making it less prone to spontaneous ignition. Despite these favorable properties, liquid ammonia is highly toxic, and its vapor pressure at ambient temperature is approximately three orders of magnitude greater than that of gasoline or methanol, increasing its potential hazard in terms of toxicity.

Despite its relatively narrow flammability limits (15.15–27.35% in air) and high auto-ignition temperature (651 °C), ammonia is still capable of producing violent explosions under confined or poorly ventilated conditions when mixed within its flammable range.

The minimum ignition energy (MIE) of ammonia vapor is approximately 680 mJ significantly higher than that of hydrogen (0.02 mJ) or methane (0.28 mJ) which means ammonia generally requires stronger ignition sources to initiate combustion. However, once ignited in a confined space, it can generate substantial overpressures due to its low laminar flame speed (~0.07 m/s) and high combustion energy release.

Historically, several severe industrial accidents have underscored the explosive potential of ammonia under specific conditions. For example, the Texas City disaster (1947) [46] involved the detonation of ammonium nitrate aboard a ship, indirectly highlighting ammonia's hazardous decomposition potential. More directly, the 1948 Cleveland [47] ammonia explosion caused by a leak from a pressurized pipeline led to multiple fatalities and extensive damage, emphasizing the critical importance of leak detection and ventilation in storage and transport systems. Additionally, in 2004 [48], a tank rupture at an ammonia storage facility in Belgium caused a major release, triggering fire and blast hazards in nearby industrial complexes. Such incidents serve as a stark reminder that, although ammonia is not as easily ignitable as some other fuels, under specific conditions particularly in enclosed or semi-enclosed environments, it poses a considerable explosion hazard. Therefore, its use as a marine fuel demands rigorous risk assessments, explosion modeling, and safety system integration, particularly in confined areas like engine rooms or fuel preparation compartments aboard ships.

2.2. Hazards Associated with Ammonia in Fuel Gas Supply Systems (FGSS)

The hazards associated with ammonia can be categorized into three primary aspects: (i) its toxic effects, (ii) its corrosive properties, and (iii) its flammability risks.

2.2.1. Toxicological Effects of Ammonia on Humans

Ammonia is a colorless, toxic gas characterized by a strong, pungent odor detectable at concentrations between 5 and 30 ppm. Being less dense than air, it disperses rapidly; however, liquid ammonia poses serious hazards, capable of causing severe chemical burns and tissue damage upon skin contact. Large-scale ammonia releases carry a significant risk of fatality, as the gas can form a toxic cloud that travels far from the leak site, potentially exposing individuals at a distance. Deaths typically occur from inhaling high concentrations or being trapped in confined spaces without escape, despite ammonia's intense odor serving as a warning at levels well below harmful concentrations. Ammonia readily dissolves in water, and exposure to anhydrous ammonia can lead to dehydration of tissues and chemical burns through the formation of ammonium hydroxide. Furthermore, when liquid ammonia vaporizes, it rapidly absorbs heat from the skin and underlying tissues, causing frostbite within seconds.

The likelihood of fatality resulting from the dispersion of an ammonia vapor cloud leak can be estimated by [49]

$$P_{d\_toxic} = P_d \tag{1}$$

where P_{d_toxic} denotes the probability of human fatality due to toxic exposure to ammonia, and P_d represents the overall probability of human death.

$$P_d = 0.5[1 + \text{erf}(\frac{P_r - 5}{\sqrt{2}})] \tag{2}$$

$$P_r = (-15.6)(\ln(C^2 \times t)) \tag{3}$$

$$\text{erf}(x) = \frac{2}{\sqrt{\pi}} \int_0^x e^{-t^2} dt \tag{4}$$

Here, *t* denotes the exposure duration, *C* represents the concentration of the ammonia vapor cloud (measured in mg/m^3), and erf(x) refers to the Gaussian error function.

It is important to recognize that ammonia's toxic effects can accumulate over time; repeated exposure to even low concentrations may lead to serious health issues. Consequently, strict safety measures such as using proper personal protective equipment (PPE) and ensuring adequate ventilation are crucial to minimize the risk of harmful exposure.

2.2.2. Environmental Impact of Ammonia Toxicity

Ammonia leaks into seawater during bunkering operations can have devastating consequences for marine ecosystems [50]. The rapid absorption of ammonia by water can quickly reach lethal concentrations, leading to the immediate death of aquatic organisms in the vicinity. Additionally, ammonia reacts exothermically with water and tends to vaporize quickly. As a gas lighter than air, it ascends into the atmosphere, forming a hazardous vapor cloud.

This airborne ammonia cloud remains a critical threat to surrounding life, especially during its initial dispersion [51]. Even as it dilutes through mixing with ambient air, the gas may still expose nearby organisms to harmful concentrations. The potential for harm persists throughout the evaporation and dispersion process.

To mitigate environmental risks, strict measures must be implemented to prevent the unintentional release of ammonia [52]. These include well-ventilated storage systems, secure handling procedures, responsible disposal practices, and cautious application of ammonia-based substances such as fertilizers.

2.2.3. Combustion and Flammability Characteristics of Ammonia

Ammonia possesses an auto-ignition temperature of approximately 651 °C under standard atmospheric conditions and exhibits a narrow flammability range of 15.15% to 27.35% by volume in air. Compared to conventional fuels, its ignition risk is significantly lower, primarily due to its relatively high minimum ignition energy of around 680 mJ approximately 2000 times greater than that of methane. Despite its low flammability under normal conditions, ammonia leaks from high-pressure storage systems can be hazardous. As a gas lighter than air, it disperses rapidly, potentially increasing the risk of exposure and secondary hazards.

With the growing utilization of hydrogen in industrial applications such as fuel storage, refrigeration, and exhaust gas treatment, there is a heightened need for robust fire safety protocols when ammonia is involved. Like other hydrocarbons, liquid-phase ammonia does not sustain combustion without an external heat source. This is due to insufficient heat feedback from the flame to the liquid pool. However, if ammonia comes into contact with a heated surface such as soil or water, sufficient vaporization may occur to support a sustained fire.

The primary hazards associated with ammonia bunkering involve the risk of fire and explosion, particularly when accidental releases or leaks occur near ignition sources (Figure 1). In the absence of ignition, ammonia will vaporize and form a gas cloud that gradually disperses into the atmosphere. However, if ignition occurs, four major fire and explosion scenarios can arise: vapor cloud flash fire, jet fire, pool fire, and vapor cloud explosion. The severity of these events is influenced by variables such as the initial temperature and chemical composition of the released ammonia, as well as the size of any resulting liquid pool.
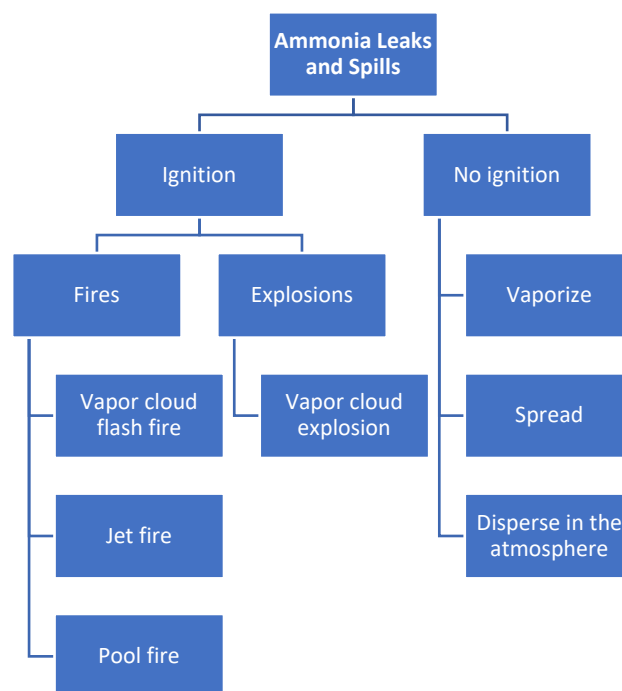
Figure 1. Main hazard of an ammonia bunkering process.

Compared to fuels like LNG and LPG, ammonia presents a lower fire hazard due to its relatively slow combustion rate. For firefighting, large ammonia fires can be effectively controlled using water sprays, mist, or foam, while small-scale fires are better managed with dry chemical agents or carbon dioxide. It is critical to avoid applying a direct water stream onto ammonia leaks or spills, as this can trigger hazardous chemical reactions. Emergency personnel should always use fully encapsulated protective gear with a self-contained breathing apparatus (SCBA), even when ammonia concentrations are as low as 25 ppm, due to the compound's high toxicity and corrosive nature.

2.2.4. Corrosive Characteristics of Ammonia

Ammonia is a chemically active compound capable of causing significant corrosion and degradation to various materials, including metals, plastics, and rubber. Its corrosive nature arises primarily from its reaction with water, forming ammonium hydroxide a strongly alkaline solution that can aggressively attack susceptible surfaces. The following outlines how ammonia affects different materials:

Metals: Ammonia can induce corrosion in metals, especially those lacking resistance to alkaline environments. Upon contact, it may lead to surface pitting, discoloration, or accelerated deterioration of metal structures. Over time, this corrosion compromises structural integrity, potentially resulting in mechanical failure or leakage.

Plastics: Certain plastics, particularly those not designed to withstand high pH levels, are vulnerable to ammonia exposure. Interaction with ammonia can cause these materials to become brittle, develop cracks, or lose their mechanical strength. Components under continuous mechanical stress or pressure are especially at risk of premature failure.

Rubber: Ammonia can degrade rubber compounds that are not chemically resistant to alkalis. Exposure can cause rubber to soften, swell, or even disintegrate. This degradation is particularly hazardous for rubber elements used in dynamic systems involving friction, pressure, or sealing functions.

To mitigate these risks, it is essential to implement stringent safety protocols for ammonia handling and storage. This includes using materials specifically rated for alkaline resistance, applying protective coatings, and ensuring that vulnerable components are

either shielded or replaced with compatible alternatives. Proper design and maintenance practices are crucial to prevent equipment failure and ensure operational safety in ammonia-handling systems.

2.2.5. Other Hazards Related to the Use of Ammonia

Ammonia systems are particularly vulnerable to hydraulic shock due to ammonia's high boiling point and substantial volumetric expansion upon vaporization. Hydraulic shock, also known as liquid hammer, occurs when there is an abrupt change in fluid velocity within a piping system, leading to a sharp pressure spike. This pressure surge can cause serious damage to pipelines, valves, and other components. One common scenario where this may occur is during transitions between refrigerated and defrosted conditions in ammonia-based cooling systems.

In addition to internal system risks, the uncontrolled release of pressurized ammonia into the environment introduces further hazards. Upon release, approximately 8–9% of the liquid ammonia can instantly vaporize due to pressure drop, rapidly expanding in volume. Ammonia has an expansion ratio of roughly 1:710 from liquid to vapor, and even after initial depressurization, further evaporation can continue, especially when conditions favor re-boiling such as after precipitation or cooling.

A particularly dangerous scenario is the Boiling Liquid Expanding Vapor Explosion (BLEVE). This physical explosion occurs when a pressurized liquid suddenly undergoes rapid boiling due to a sudden loss of containment or pressure. For a BLEVE to occur, the temperature of the liquid must exceed its superheat limit at the time of depressurization. Although ammonia has a relatively high critical temperature of 89.8 °C well above typical ambient and storage conditions, the potential for BLEVE in ammonia systems is generally considered low under normal operating conditions. Nonetheless, proper design and maintenance are essential to prevent such rare but catastrophic failures.

3. Numerical Study of Ammonia Dispersion

3.1. Simulation Domain and Turbulence Model

In this research, a three-dimensional computational model was developed to investigate the dispersion characteristics of ammonia leakage within a marine fuel preparation room (FPR). The model was based on the actual geometry of a representative FPR with dimensions of 11 m × 16 m × 0.6 m, structurally divided into 06 panel upper and lower decks and other fours walls includes equipment such as pumps, gas supply pipelines, and compressors. The coordinate origin of the simulation domain was defined at the lower-left corner of the FPR, as shown in Figure 2. The study assumed a leakage scenario in which ammonia, after undergoing vaporization, escaped from a pipeline on the lower deck. The leak was initiated at the spatial coordinates, simulating a continuous release of ammonia into the confined FPR environment, as illustrated in Figures 2 and 3.

The mathematical framework governing fluid dynamics in this study comprises the continuity equation, the Navier–Stokes equations for momentum conservation, and the energy conservation equation. In cases where the flow involves the transport and interaction of multiple species, the analysis must additionally satisfy the species (or component) conservation equations to accurately capture mixing and diffusion phenomena.
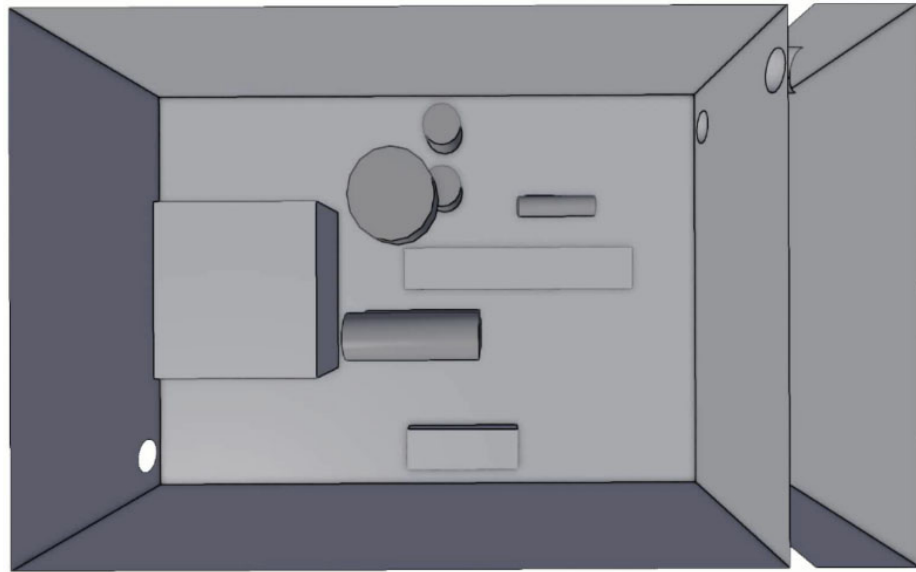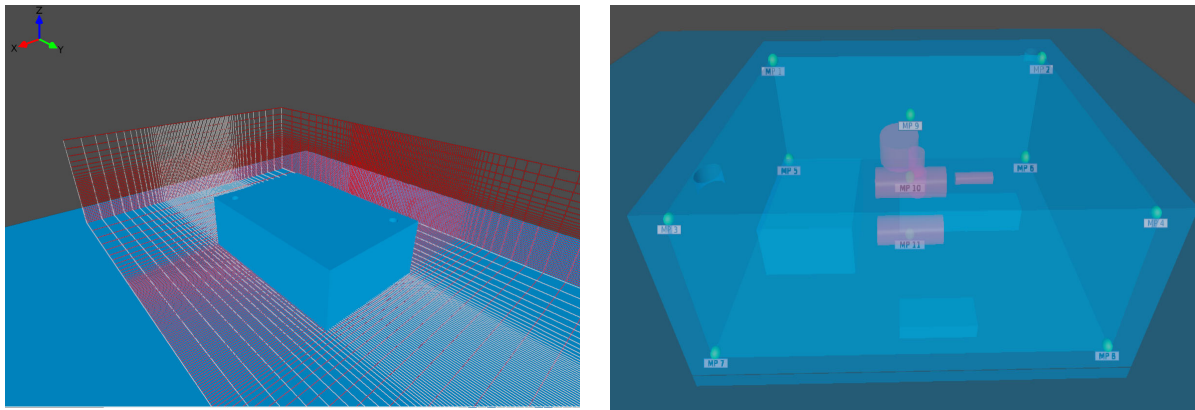
Figure 2. Fuel preparation room.

Figure 3. Simulation domain.

Mass conservation principle:

$$\frac{\partial}{\partial t}(\beta_\vartheta \rho) + \frac{\partial}{\partial x_j}(\beta_j \rho u_j) = \frac{m}{V} \tag{5}$$

where β_j, β_ϑ denote porosity and volume porosity, u_j denotes mean velocity (m/s), m, ρ, V represent the mass rate (kg/s), density (kg/m^3), and volume (m^3), respectively.

Momentum conservation principle

$$\frac{\partial(\rho u_j)}{\partial t} + \frac{\partial}{\partial x_j}(u_i \rho u_j) = -\frac{\partial p}{\partial x_j} + \frac{\partial}{\partial x_j}\left(\mu \frac{\partial u_i}{x_j}\right) + \rho g + F_i \tag{6}$$

Energy conservation principle:

$$\frac{\partial \rho h_s}{\partial t} + \nabla(\rho u h_s) = \frac{Dp}{Dt} - \nabla \dot{q}'' + \tau \nabla \mathbf{u} \tag{7}$$

Standard k-ε model transport equation:

$$\frac{\partial}{\partial t}(\rho K) + \frac{\partial}{\partial x_j}(\rho K u_i) = \frac{\partial}{\partial x_j}\left[\left(\mu + \frac{u_t}{\sigma_k}\right)\frac{\partial k}{\partial x_j}\right] + G_k + G_b - \rho\varepsilon - Y_M + S_b \tag{8}$$

The gas leakage rate at the defined release point will be evaluated based on fluid dynamic principles and appropriate boundary conditions [53–55]:

$$Q = C \times A \times \rho_L \sqrt{\frac{2(P_T - P_{atm})}{\rho_L} + 2gH} \tag{9}$$

In this analysis, the initial leakage rate Q (kg/s) is calculated using an orifice flow model, where A denotes the cross-sectional area of the leakage orifice (m^2), and ρL represents the density of the stored cryogenic fluid as ammonia (NH_3). The term C refers to the discharge coefficient, which accounts for flow contraction and frictional effects at the orifice and is set to 0.62 for a sharp-edged opening. The pressure differential driving the flow is given by the difference between the internal fluid pressure in the pipeline PT and the ambient atmospheric pressure P atm, both expressed in pascals (Pa). Gravitational acceleration is denoted by $g = 9.81$ m/s^2, while H represents the vertical height between the surface level of the liquid pool and the centerline of the leak orifice, influencing the hydrostatic pressure contribution to the leak rate.

The leakage and dispersion of ammonia are governed by complex turbulent flow dynamics. Accurately capturing the behavior and distribution of gas during these processes requires the selection of an appropriate turbulence modeling approach. FLACS-CFD V12.2. offers a range of turbulence models, among which the k-ε family (including the Standard, RNG, and Realizable k-ε models) is commonly employed in gas flow simulations. Comparative analyses across these models have demonstrated that the Realizable k-ε model provides superior accuracy in representing the diffusion characteristics of light gases such as ammonia. Consequently, this study adopts the Realizable k-ε model for all computational simulations related to ammonia leakage and dispersion. The application of FLACS-CFD simulations, particularly using the k-ε turbulence model, has been widely validated by numerous researchers for accurately modeling ammonia dispersion and explosion phenomena. For instance, Tan et al. [33] investigated ammonia dispersion behavior in a food processing facility using both small-scale wind tunnel experiments and FLACS-CFD simulations. Their findings demonstrated that the RNG k-ε turbulence model yielded results that closely matched the experimental data, effectively capturing the sharp concentration gradients and illustrating how horizontal wind flow governs ammonia dispersion patterns. Similarly, Liu et al. [56] focused on the critical ship-to-ship ammonia bunkering process by employing CFD simulations to evaluate various leakage scenarios under different leak orientations and wind directions. Due to the complexity and variability of dispersion behaviors in maritime environments, and the limitations of traditional Gaussian dispersion models, the study strongly advocates for conducting vessel-specific CFD analyses to ensure the safety and reliability of ammonia bunkering operations. Bae et al. [32] explored the impact of ignition source location on the explosion behavior of ammonia within a fuel preparation room, employing CFD simulations using the FLACS platform. A total of nineteen ignition scenarios were systematically evaluated across the X-, Y-, and Z-axes to capture a comprehensive range of potential ignition points. The simulation outcomes showed strong agreement with experimental data and offered valuable insights for the risk assessment and safety optimization of ammonia-fueled marine systems. These findings underscore the importance of ignition positioning in determining explosion severity and support the development of safer design strategies for future ammonia-based propulsion technologies.

The simulation domain is presented in Figure 3. The boundary condition and initial condition for study case are presented in Tables 2 and 3.

Table 2. Boundary conditions.

Boundary Condition	
XLO	Euler
XLO	Euler
YLO	Euler
YHI	Euler
ZLO	Euler
ZHI	Euler

Table 3. Initial conditions of case study.

Initial Condition	
Ambient pressure [Pa]	101,325
Environment temperature [K]	288.15
Gas composition ratio	Ammonia 100%
Gas cloud volume	Equivalent volume (ER = 1)
Shape of cloud volume	$10 \times 15 \times 5$ cube

3.2. Grid Dependence

To accommodate the complex geometry of the model, unstructured meshes were employed along the external surfaces, allowing for greater flexibility in capturing irregular shapes. In contrast, structured grids were utilized within the internal flow domains to optimize both numerical accuracy and computational efficiency. Additionally, localized mesh refinement was implemented in the vicinity of the leakage source to ensure high-resolution simulation of critical flow characteristics.

A grid convergence study was conducted using the standard k-ε turbulence model to ensure mesh independence and numerical accuracy. Five different grid resolutions were evaluated within the leakage region, with cell sizes of 0.05 m, 0.1 m, 0.2 m, 0.4 m, 0.5 m, and 1 m applied in the x and y directions, while maintaining a constant cell size of 0.4 m in the z direction. Outside the leakage zone, the mesh was gradually coarsened using a grid expansion ratio of 1.15 to optimize computational efficiency without compromising accuracy.

As shown in Figure 4, the results of the convergence analysis confirmed that the 0.1 m mesh resolution within the core region provided a suitable balance between computational cost and solution accuracy. Therefore, this resolution was adopted for subsequent simulations. The final mesh configuration consisted of approximately 308,880 cells.
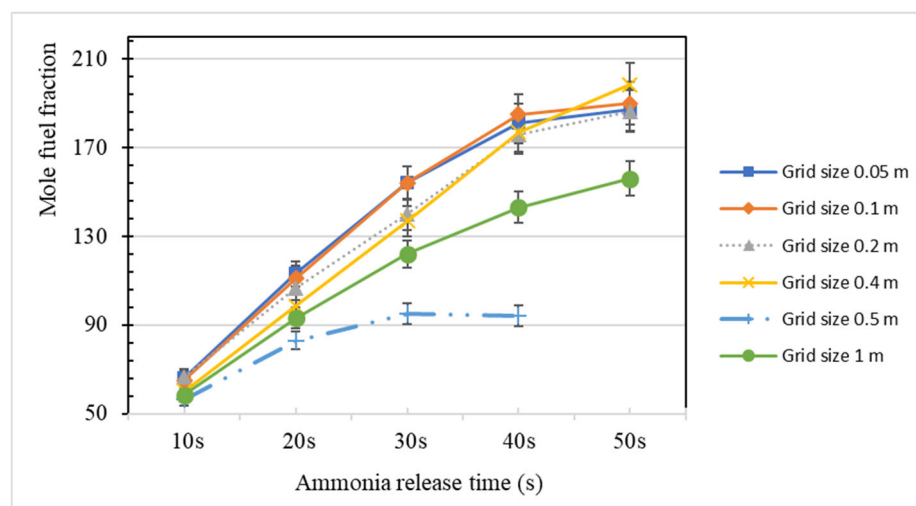
Figure 4. Grid dependence.

3.3. Dispersion of Ammonia

To investigate the leakage and dispersion behavior of ammonia within the FPR, 11 monitoring points (MP) were strategically positioned to measure gas concentration at various locations, as detailed in Table 4. The MPs works as sensor for recording the variable of pressure, temperature, velocity, and other parameters as required. Given that ammonia has a flammability range between 15% and 27% by volume in air, the initial analysis primarily considered gas concentrations within this explosive range. However, ammonia is not only flammable but also highly toxic. Human health can be adversely affected by concentrations as low as 25 ppm, which is typically considered the threshold for minimal health effects according to occupational exposure guidelines (e.g., ACGIH TLV, OSHA PEL).

Table 4. MPs arrangement in the simulation domain.

Monitor Point	Monitor Point		
	X	Y	Z
MP1	0.1	0.1	4.9
MP2	0.1	14.9	4.9
MP3	9.9	0.1	4.9
MP4	9.9	14.9	4.9
MP5	0.1	0.1	0.1
MP6	0.1	14.9	0.1
MP7	9.9	0.1	0.1
MP8	9.9	14.9	0.1
MP9	5	7.5	4.9
MP10	5	7.5	2.5
MP11	5.2	7.5	0.1

To comprehensively evaluate the impact of ammonia dispersion including effects on human health, environmental safety, and equipment integrity, the scope of the analysis was expanded. Rather than limiting the investigation to concentrations within the flammable range (15–27%), the lower boundary was extended down to 25 ppm. This extended range (25 ppm to 27%) allows for a more holistic assessment of both toxic and flammable hazards associated with ammonia releases, capturing the full spectrum of potential risk scenarios during storage, handling, and accidental release.

Figure 5 presents the three-dimensional concentration distributions, along with vector and contour plots, at different leakage time intervals. In the early stages of dispersion, the low molecular weight of ammonia, coupled with buoyancy effects and air resistance, leads to a characteristic umbrella-shaped distribution pattern. As time progresses, gas accumulation increases, and air resistance becomes less influential, resulting in a transition to a cone-shaped dispersion profile.

To comprehensively analyze the dispersion characteristics of ammonia leakage in the confined space of FPR, five potential leak directions are considered: +X, −X, +Y, −Y, and +Z. These directions represent different orientations of possible pipe ruptures or equipment failures and are chosen to evaluate how the initial direction of the ammonia jet affects its behavior within the room. When a leak occurs, ammonia is typically stored or transported under pressure, and the sudden pressure differential between the inside of the pipe and the ambient environment causes a rapid jet release of ammonia vapor in the direction of the breach. This high-velocity jet is the primary driver of the initial dispersion, with its path and momentum strongly influenced by the leak orientation.
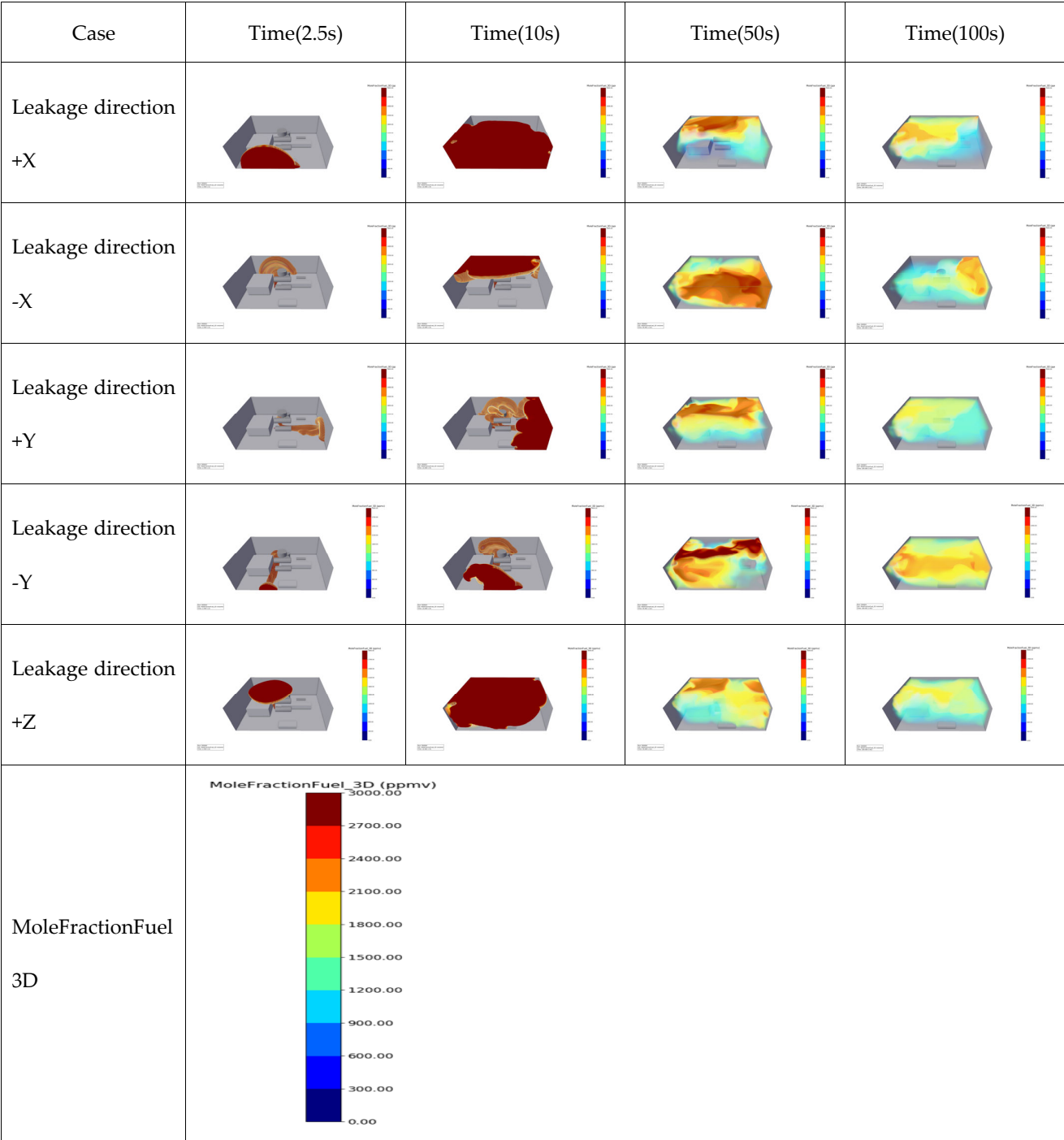
Figure 5. Ammonia dispersion in FPR according to time release.

During the initial diffusion phase, particularly around t = 2.5 s and t = 10 s, the gas jet interacts with several physical barriers including the upper left wall, the first row of equipment, and the rear bulkhead leading to localized accumulation. In these regions, concentrations can reach approximately 14%. The presence of such obstacles impedes the momentum of the gas, slowing its velocity and effectively reducing downstream concentrations while limiting outward dispersion.

Following this initial phase, the ammonia vapor begins to interact with the surrounding environment. Due to the heat exchange between the cold ammonia jet and the warmer air and surfaces within the FPR, additional vaporization may occur, especially if the ammonia was initially in liquid form. This thermal interaction, along with the geometric

complexity of the FPR, including the presence of machinery, walls, and structural elements, contributes to the turbulent mixing and uneven distribution of ammonia within the room. The shape and layout of the equipment can create localized eddies and stagnation zones where ammonia may accumulate. Furthermore, since ammonia is denser than air, it tends to sink and spread along the lower regions of the space, which increases the risk of prolonged exposure in areas not effectively ventilated.

The direction of the leak plays a critical role in determining how quickly and effectively the ammonia disperses. In the +X and −X directions, the influence of the ventilation system is significant, as the air exchange and flow are aligned with these axes. This facilitates faster dilution and removal of the leaked gas, resulting in shorter dispersion times and reduced concentration levels compared to other directions. In contrast, leaks in the ±Y directions occur perpendicular to the primary ventilation flow, leading to slower dispersion and greater accumulation of ammonia in zones with limited airflow. Additionally, a leak in the +Z direction pointing upward can cause the vapor to rise initially, potentially reaching the ceiling or upper structures, where it may stagnate or later descend due to gravity. This bidirectional movement increases the risk of gas accumulation in both elevated and lower areas, especially in poorly ventilated sections.

By t = 50 s, high-concentration gas begins to occupy the first and second layer zones. The closed configuration of the FPR's upper exhaust channel results in significant gas buildup in this area. The changing of mole fraction fuel in response with ammonia release is shown in Table 5.

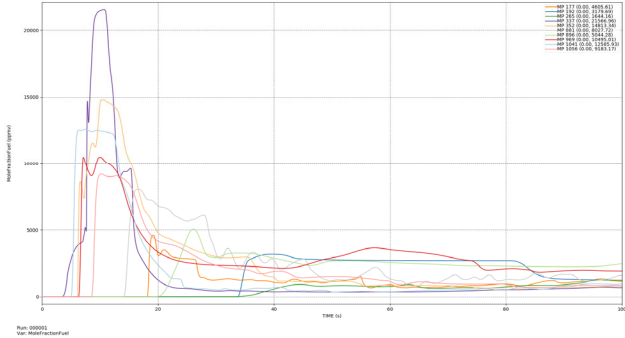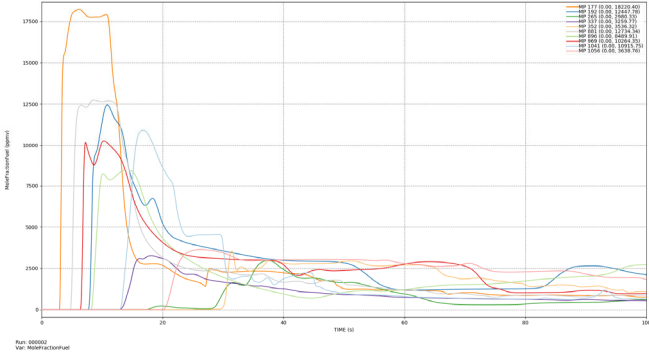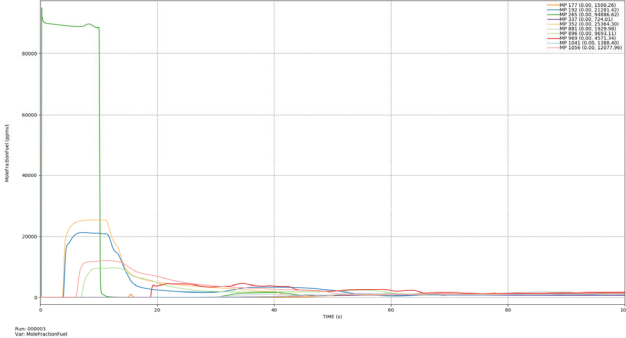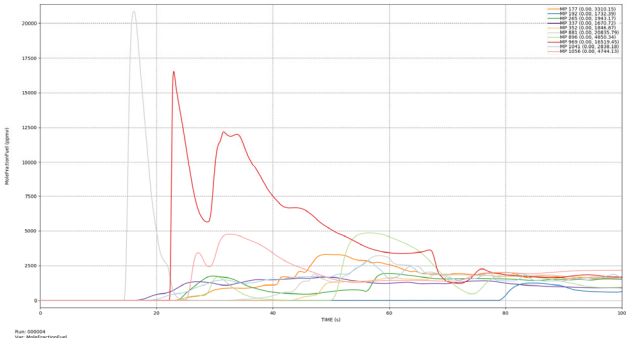**Table 5.** Changing of mole fuel fraction of ammonia release.
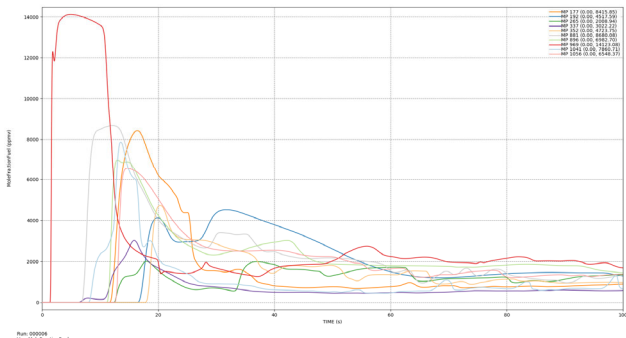
Case	Mole Fraction of Fuel at Monitoring Points According to Leak Rate	Order of Detection and Time			
		Order of Detection (25 ppm)	Time (s)	Order of Detection (300 ppm)	Time (s)
Leakage direction +X		337	3.59	337	3.93
		1041	5.03	1041	5.13
		352	6.11	352	6.15
		969	6.32	969	6.41
		1056	8.57	1056	8.68
		881	14.14	881	14.30
		177	18.20	177	18.27
		896	20.08	896	20.97
		192	33.80	192	34.10
		265	34.16	265	37.84
Leakage direction −X		177	2.95	177	2.99
		881	4.79	881	4.87
		969	6.42	969	6.51
		192	7.78	192	7.88
		896	8.21	896	8.35
		1041	12.98	1041	13.20
		337	13.03	337	13.60
		265	17.67	1056	20.69
		1056	20.23	265	28.95
		352	29.26	352	30.18

Table 5. *Cont.*

Case	Mole Fraction of Fuel at Monitoring Points According to Leak Rate	Order of Detection and Time			
		Order of Detection (25 ppm)	Time (s)	Order of Detection (300 ppm)	Time (s)
Leakage direction +Y		265	0.16	265	0.18
		352	3.70	352	3.77
		192	3.89	192	3.94
		1056	6.04	1056	6.13
		896	6.90	896	7.00
		177	15.09	177	15.22
		969	18.82	969	18.89
		881	24.02	881	31.39
		337	30.55	337	40.22
		1041	33.05	1041	40.94
Leakage rate of −Y		881	14.44	881	14.55
		337	16.83	337	19.03
		1041	19.08	1041	21.61
		969	22.21	969	22.29
		177	23.43	265	24.55
		265	23.90	1056	25.38
		896	23.93	896	26.00
		1056	25.01	177	26.83
		352	43.51	352	46.02
		192	79.08	192	79.87
Leakage direction +Z		969	1.42	969	1.45
		337	6.56	881	7.06
		881	6.88	1041	8.38
		1041	8.10	337	11.09
		896	11.23	896	11.42
		177	11.76	177	12.00
		265	12.50	1056	12.79
		1056	12.60	265	12.80
		192	16.64	192	16.97
		352	17.94	352	18.21

In the later stages of diffusion, particularly after t = 50 s, critical regions such as the equipment vicinity and the rear of the FPR aligned with the primary direction of the gas jet experience concentrations approaching the 14% LEL, making them the most hazardous zones. Conversely, the sidewalls remain the least affected, maintaining concentrations below 25 ppm, largely due to their greater distance from the source and the flow-interrupting effect of the equipment layout.

To thoroughly assess gas distribution and inform the development of evacuation strategies and ignition prevention zones, concentration calculations were performed on

the 11 designated monitoring planes. Table 5 presents the temporal variation in ammonia fuel mole concentration at 11 monitoring points strategically placed throughout the FPR. These monitoring points are used to evaluate how ammonia disperses under different leakage directions, offering insights into spatial and temporal concentration gradients within the confined environment. For each leakage direction +X, −X, +Y, −Y, and +Z the time-dependent changes in ammonia concentration reveal distinct dispersion patterns influenced by leak orientation, sensor location, equipment layout, and ventilation design. In the +X and −X leakage cases, significant fluctuations in fuel mole concentration are observed primarily between 5 and 20 s after the onset of leakage. This can be attributed to the alignment of these directions with the mechanical ventilation system, which promotes rapid airflow and early detection at the monitoring points, resulting in sharp but short-lived concentration peaks.

In contrast, the +Y and +Z leak directions exhibit a more immediate rise in ammonia concentration, with critical levels occurring within the 0–18 s of release. These directions are less aligned with the main ventilation flow, causing the ammonia to disperse more freely and quickly reach the surrounding sensors without immediate removal. The +Z direction, in particular, leads to vertical dispersion toward the ceiling, where the gas may accumulate before gradually spreading downward due to gravity, impacting sensors at both high and low positions. The most critical dispersion behavior is observed in the −Y direction, where fuel mole concentration remains elevated for an extended period, notably from 5 to 40 s. This prolonged exposure is mainly due to three factors: first, the leak occurs on the side opposite to the primary ventilation flow, limiting the removal efficiency; second, the physical arrangement of equipment in this area obstructs airflow and promotes accumulation; and third, the sensor placement in this region captures delayed yet sustained gas presence due to the recirculating flow patterns. Together, these findings highlight the strong influence of leakage direction on ammonia dispersion dynamics and underscore the importance of optimizing both sensor placement and ventilation layout to ensure early detection and effective mitigation of toxic gas release events.

Overall, examining ammonia leakage in multiple directions enables a comprehensive understanding of how leak orientation, room geometry, thermal effects, and ventilation interact to influence gas dispersion. This insight is critical for optimizing sensor placement, emergency ventilation activation, and safety protocols to minimize toxic exposure and explosion risks in confined marine or industrial environments.

3.4. Ammonia Dispersion with Different Release Rate

To investigate the influence of leakage rate on ammonia dispersion within the FPR, five different leakage scenarios were considered: 0.1 kg/s, 0.5 kg/s, 1.0 kg/s, 5.0 kg/s, and 10.0 kg/s. As expected, higher leakage rates result in a greater total mass of ammonia being released over the same time period. However, the dispersion behavior is not solely governed by the leakage rate. Factors such as ambient temperature, ventilation conditions, and heat flux significantly affect the spread and distribution of ammonia within the room. For example, higher heat flux may enhance buoyancy-driven flow, potentially accelerating upward dispersion, while poor ventilation could lead to localized accumulation. The variation in ammonia mole fraction across different leakage rates is illustrated in Figure 6, demonstrating how increasing release rates influence concentration gradients and spatial distribution patterns within the FPR.
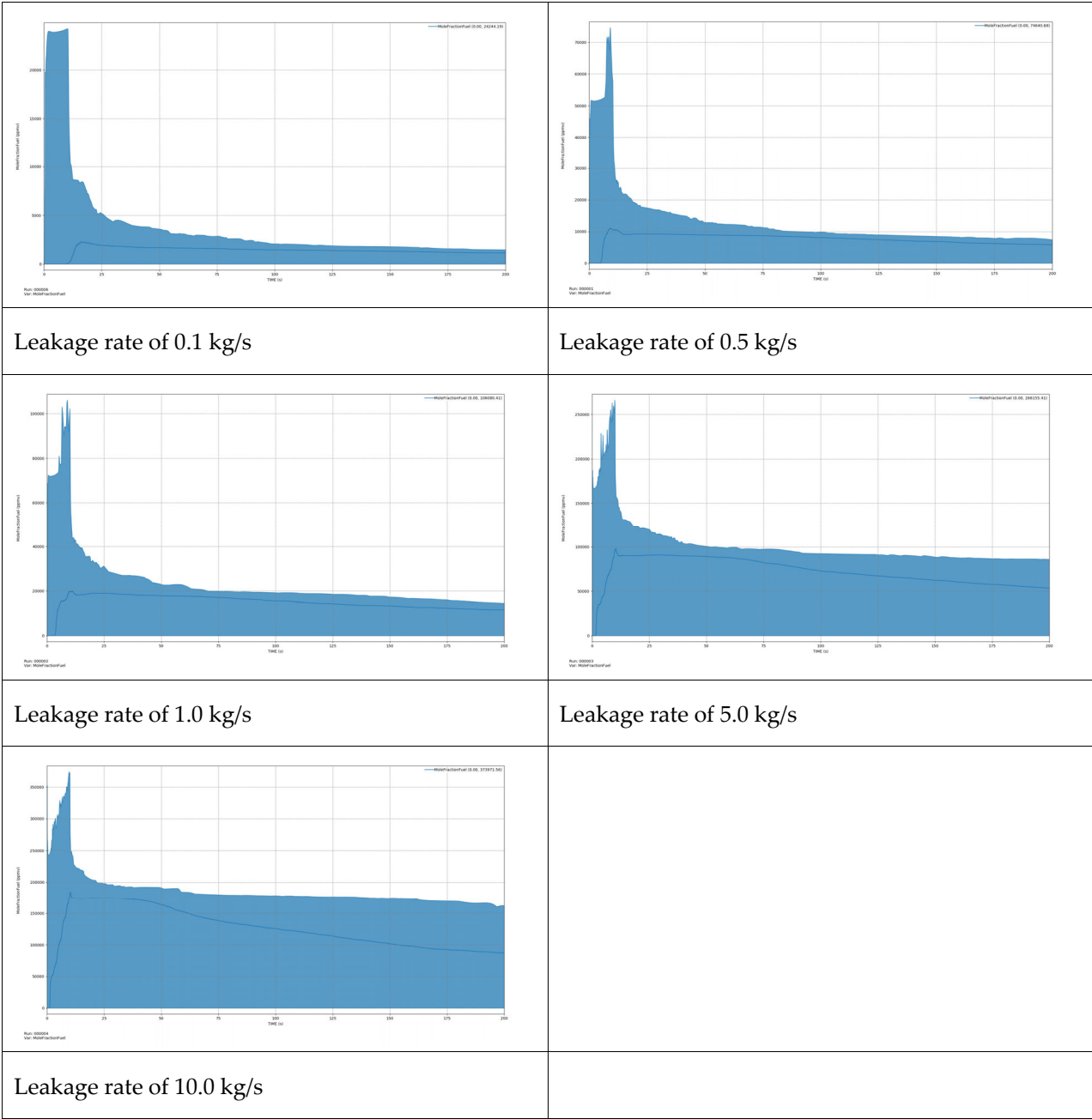
Leakage rate of 0.1 kg/s	Leakage rate of 0.5 kg/s
Leakage rate of 1.0 kg/s	Leakage rate of 5.0 kg/s
Leakage rate of 10.0 kg/s	

Figure 6. Changing of mole fuel fraction with different leakage rate.

As illustrated in Figure 7, under a small leakage rate, the dispersion of ammonia occurs more rapidly due to the accelerated vaporization process. This is primarily because ammonia has a high vapor pressure at ambient temperatures, allowing it to transition quickly from liquid to gas upon release.

In confined spaces, ammonia tends to rise due to its lower density compared to air. The vapor follows an upward trajectory and may accumulate in elevated zones, particularly at structural intersections such as corners formed by walls and surrounding equipment. These corners act as barriers, limiting airflow and allowing ammonia gas to stagnate, leading to localized concentrations. This accumulation increases the risk of exposure for personnel and poses potential hazards to nearby sensitive equipment if not properly ventilated.
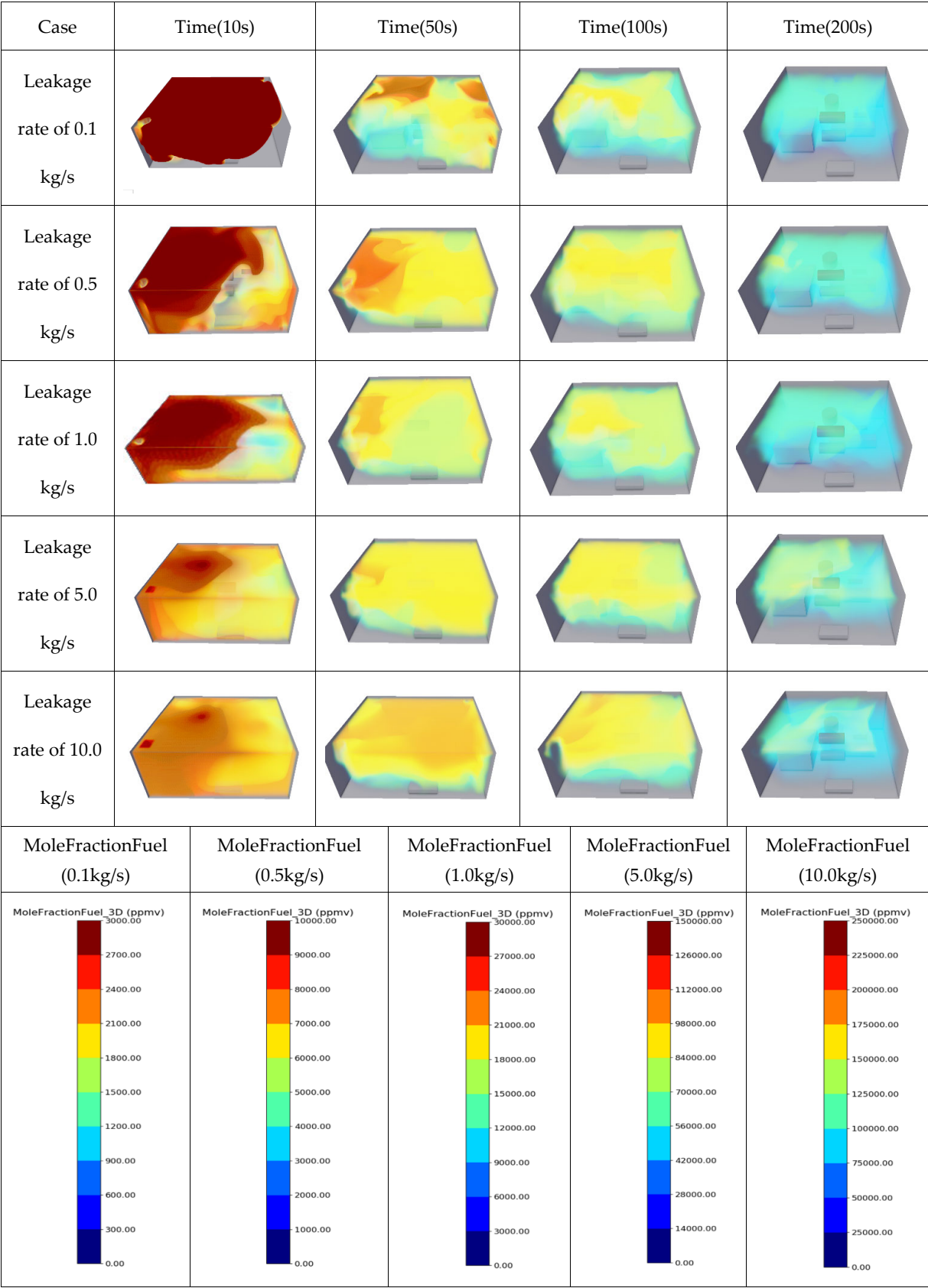
Figure 7. Three-dimensional Mole fraction of ammonia according to leak rate.

Average and peak ammonia concentrations in the FPR at 200 s according to leak rates are presented in Table 6.

Table 6. Maximum concentration of Ammonia in FPR.

Case	Maximum Ammonia Concentration (ppm)	Average Ammonia Concentration After 200 s (ppm)
Leakage rate of 0.1 kg/s	24,244.19	1135.78
Leakage rate of 0.5 kg/s	74,640.68	5841.35
Leakage rate of 1.0 kg/s	106,080.41	11,554.08
Leakage rate of 5.0 kg/s	266,155.41	53,416.11
Leakage rate of 10.0 kg/s	373,971.56	87,136.67

Based on this detailed analysis, caution zones and safe evacuation routes were established. Due to the obstructive influence of equipment on gas dispersion, appropriate barriers are proposed near the leakage source to contain the spread. Personnel should avoid areas surrounding obstacles where gas accumulation is likely to be highest. Emergency egress should follow designated pathways leading toward the sidewalls the safest regions within the FPR while avoiding high-risk zones along the gas jet trajectory and near equipment and rear compartments.

4. Ammonia Explosion

4.1. Explosion Modeling

Ammonia explosions fall under the category of chemical explosions and require the fulfillment of three fundamental conditions: (1) the presence of ammonia gas within its flammable concentration range, (2) an adequate amount of oxidizer typically atmospheric oxygen, and (3) an ignition source with energy exceeding the minimum ignition threshold. From the previous simulation results, the peak ammonia concentration occurs in the direction of the gas jet, surpassing the lower explosive limit (LEL) of 14% by approximately t = 100 s.

To model a potential ignition event, a spherical ignition region is introduced at a uniform initial temperature of 300 K (as in Figure 8). This region is centered on the plane Z = 0.1 m at the spatial coordinates. For the purposes of simulation, it is assumed that the engine room is uniformly filled with a flammable ammonia—air mixture at the stoichiometric ratio, which represents the most reactive composition for combustion and ensures maximum energy release during ignition.

To capture the pressure propagation characteristics following ignition, monitoring points are distributed throughout the FPR from 0 m to 16 m. Due to the steep pressure gradients expected near the ignition source, denser sampling is applied within the first 20 m, with pressure sensors placed at 0.1 m intervals. Beyond this region, a 2 m spacing is adopted. In total, 11 monitoring points are deployed, as detailed in Table 2.

Given the chemical complexity of explosion phenomena, a suitable combustion model is required in addition to solving the governing conservation equations. In this study, the laminar finite-rate/turbulence-chemistry interaction model within the general finite-rate framework is employed to represent the explosion process. Although ammonia explosion involves multiple intermediate reactions, a one-step, irreversible global reaction mechanism is used for simplification, ensuring computational efficiency while maintaining sufficient accuracy for explosion dynamics analysis.
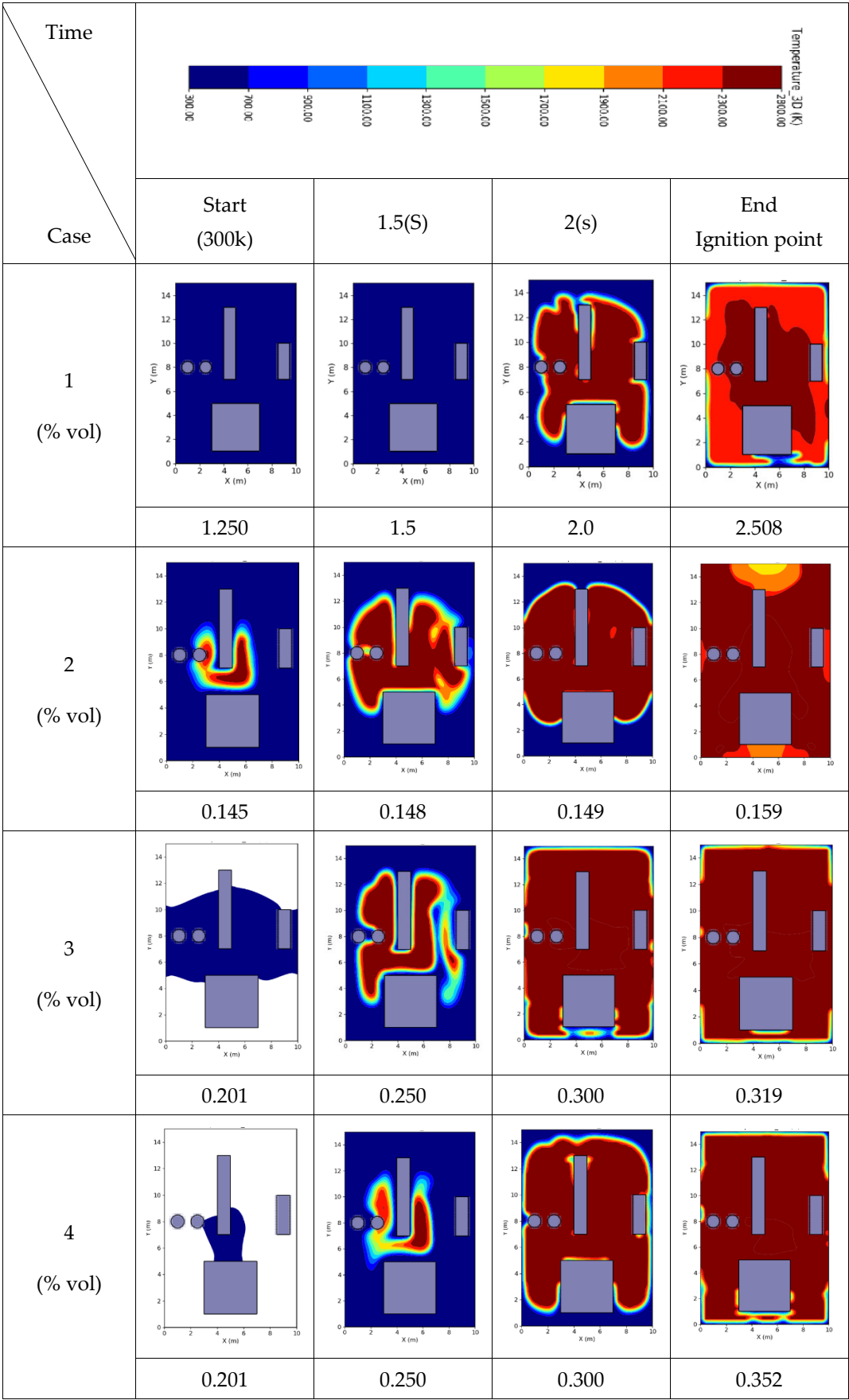
Figure 8. Temperature variation in ammonia with varying gas volume (0.1m).

4.2. TNO Multi-Energy Method

Although CFD methods offer high fidelity in simulating explosion dynamics, their application is often constrained by the need for detailed input data and extensive computational resources. This makes CFD less practical for scenarios where rapid risk assessment or preliminary analysis is required. In contrast, empirical approaches such as the TNO Multi-Energy (ME) model and the TNT equivalence method provide faster, more accessible alternatives. These simplified models are especially useful in early-stage design evaluations, routine engineering practices, and quick-response safety assessments where computational efficiency and ease of implementation are critical.

The TNT equivalence method estimates the effects of a vapor cloud explosion (VCE) by converting the chemical energy release into an equivalent mass of TNT, using standard blast curves to assess the resulting overpressure. While convenient, this method involves substantial simplifications; it ignores the actual geometry and volume of the vapor cloud, assumes instantaneous and uniform energy release, and neglects the temporal evolution of the blast wave. These limitations reduce its accuracy when applied to realistic VCE scenarios, especially in complex environments.

Although the TNT equivalency method remains commonly used for preliminary modeling of vapor cloud explosions due to its simplicity, it faces substantial limitations and criticisms regarding its scientific accuracy. As an improved alternative, the TNO ME method has gained broader acceptance within the engineering and safety communities for providing a more realistic representation of explosion dynamics.

The TNO ME approach models an explosion by defining an equivalent fuel–air charge, which is characterized by two primary parameters: the charge size and the explosion strength. Once these parameters are established, the corresponding blast wave characteristics at various distances can be obtained from standardized fuel–air explosion charts.

Traditionally, the TNO guidelines for selecting charge size and strength rely on conservative assumptions designed to prioritize safety. However, in scenarios where these conservative estimates produce excessively high overpressure predictions, a more refined and representative strength value can be derived by correlating model inputs with empirical data. To facilitate this process, a practical parameter combination has been developed to characterize the key initial and boundary conditions that govern explosion severity. This parameter set has been calibrated against experimental datasets, resulting in a collection of reference graphs. These graphs serve as an accessible database, enabling users to rapidly estimate appropriate charge strength values based on observed experimental trends. This enhancement allows for more accurate and context-specific assessments of vapor cloud explosion risks while maintaining usability for engineering applications.

On the other hand, the TNO ME model offers a more comprehensive and realistic framework for explosion analysis. It allows for the estimation of critical parameters such as peak overpressure, source radius, impulse, dynamic pressure, and shockwave duration. A notable advantage of the TNO ME model is its capacity to account for the influence of physical obstructions on explosion propagation. By dividing the vapor cloud into congested and uncongested regions and evaluating each with appropriate energy levels, the model captures the heterogeneous nature of real explosion environments more effectively. As a result, the TNO ME model is generally regarded as a more accurate and practical tool than the TNT equivalence method for assessing explosion hazards.

The methodology for applying the TNO ME model is detailed in the following sections:

- Estimation of Vapor Cloud Volume

According to the principles of the TNO ME model, the primary contribution to turbulence generation, flame acceleration, and shockwave amplification during a VCE arises

from the portion of the flammable gas cloud situated within congested or obstructed regions. These areas, due to the presence of equipment and structural elements, enhance turbulence and combustion intensity. The effective volume of the flammable cloud that actively participates in the explosion process is quantified using the following equations:

$$V_c = \frac{Q_{ex}}{\rho x C_s} \tag{10}$$

$$V_f = V_a - V_d \tag{11}$$

$$V_e = min\left(V_c, V_f\right) \tag{12}$$

where

VC: Total gas cloud volume (m^3)
Qex: Mass of the vapor cloud (kg)
ρ: Density of the gas cloud (kg/m^3)
Cs: Stoichiometric concentration of the fuel-air mixture (volume fraction)
Vf: Available free volume in the congested region (m^3)
Va: Total volume of the obstructed zone (m^3)
Vd: Volume occupied by equipment and pipelines in the obstructed area (m^3)
Ve: Effective vapor cloud volume within the obstructed region (m^3)

- Explosion intensity classification

The explosion intensity is quantified on a scale from 1 to 10, where higher values denote greater severity. In this study, the Kinsella classification approach is adopted, which evaluates explosion strength based on ignition energy, degree of congestion, and confinement level.

- ° Considered "strong" if it exceeds 100 MJ; otherwise, it is "weak".
- ° Classified as "strong" if obstacles in the area are spaced less than 3 m apart and occupy more than 30% of the total volume; otherwise, the obstruction is considered "weak".
- ° Assumed to exist if the vapor cloud is restricted by two or more solid surfaces; otherwise, it is considered "unconfined".

As in Figure 9, peak overpressure values at designated monitoring points were extracted from the CFD simulation results and compared against the outputs from the TNO ME method. Both methodologies exhibit similar trends: overpressure values decrease progressively with increasing distance from the explosion center and eventually stabilize. However, beyond 5 m from the source, TNO ME predictions at intensity levels 6 and 7 tend to overestimate peak overpressures relative to the CFD model, indicating potential conservatism in long-range estimations when higher intensity levels are applied.

Conversely, when intensity level 5 is applied in the TNO ME model, the estimated overpressures within the first 10 m are slightly lower than those predicted by CFD, but the alignment between both methods improves significantly at distances beyond 16 m showing an average relative deviation of less than 10%. Given that actual vapor cloud explosions often span extensive areas and considering the need for accurate but not overly conservative safety assessments, explosion intensity level 5 is deemed the most appropriate choice for subsequent safety distance calculations using the TNO ME method.
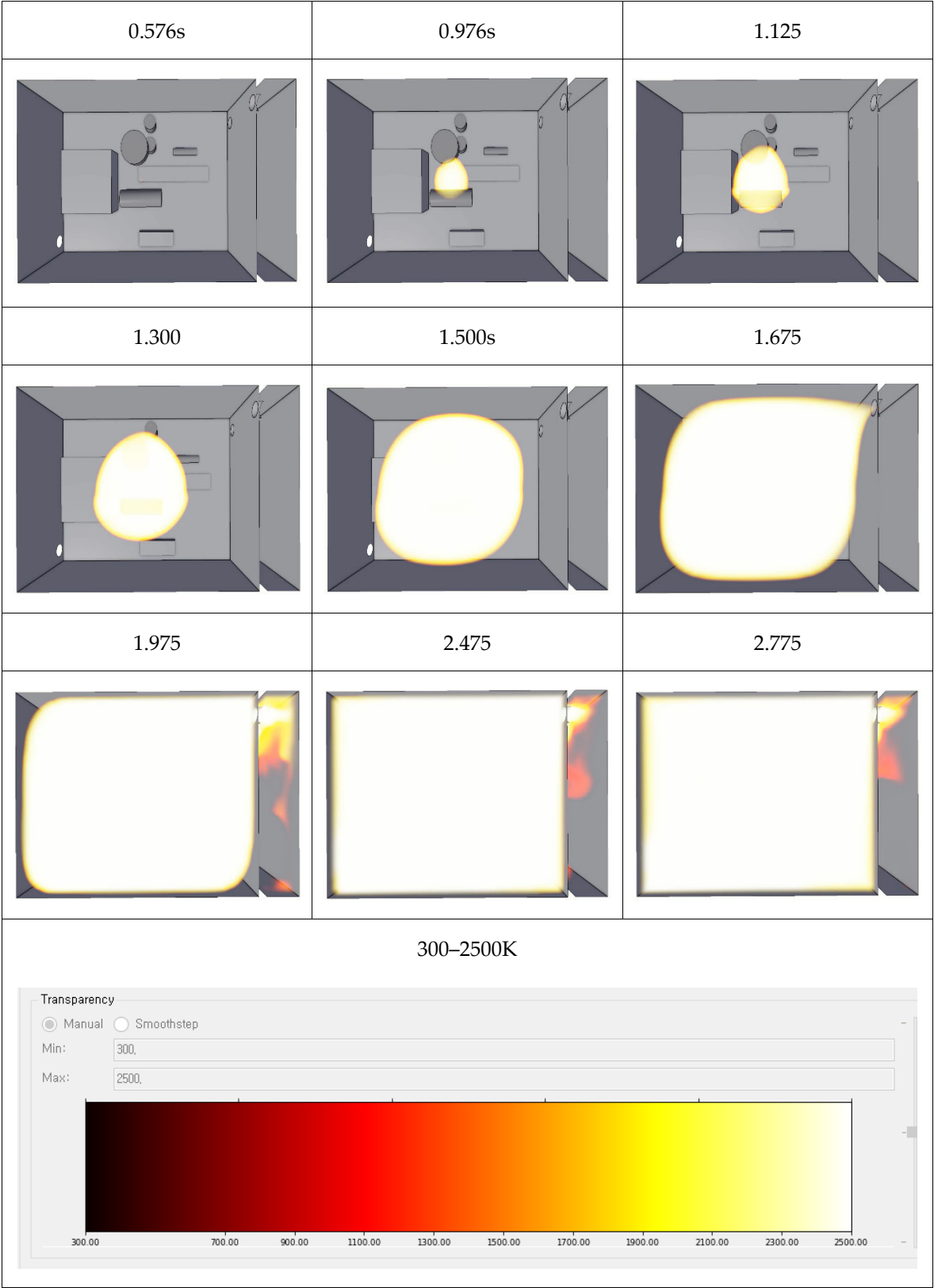
0.576s	0.976s	1.125
1.300	1.500s	1.675
1.975	2.475	2.775

300–2500K

Figure 9. Explosion rate of ammonia according to time release.

4.3. Safety Measure

For a conservative and safety-focused risk assessment, four representative overpressure thresholds were selected: 20 kPa, 30 kPa, 50 kPa, and 100 kPa. These correspond to

specific impact categories ranging from slight damage to buildings and minor injuries to individuals, up to major structural failures and life-threatening conditions.

Simulation data reveal that, within the initial 1.675 s period following an ammonia gas leak and subsequent ignition, the areas experiencing severe structural damage ($\geq$50 kPa) and zones posing a risk of serious or fatal injury ($\geq$100 kPa) remain largely confined within a 10 m radius of the explosion epicenter. However, the area where minor injuries ($\geq$30 kPa) are likely extends across the entirety of the engine room. Notably, the region susceptible to slight structural damage ($\geq$20 kPa) shows the most extensive spread, increasing from a radius of 10.51 m at 1.3 s to 15.27 m at 1.675 s post-leak approximately double the spatial extent of the minor injury zone.

Based on these observations, emergency response strategies should prioritize the rapid evacuation of personnel from high-density structural zones, as these are more vulnerable to blast-induced damage at overpressures of 50 kPa and above. Furthermore, in facilities with concentrated ammonia pipeline networks, it is highly recommended to employ blast-resistant construction materials to enhance the durability of critical infrastructure under varying levels of explosion pressure.

As the leakage duration increases, the spatial extent of critical damage or injury zones remains relatively localized. Within the first five minutes post-leakage, both fatal and severe injury zones, as well as areas susceptible to major structural damage, are confined within a 10 m radius. However, the region associated with minor injuries expands significantly, eventually encompassing the entire engine room.

As such, evacuation protocols should prioritize distancing personnel from densely constructed environments. Additionally, in regions characterized by extensive ammonia infrastructure, the implementation of blast-resistant construction materials is strongly recommended to mitigate structural vulnerabilities across varying overpressure conditions.

5. Conclusions

This study presents a comprehensive investigation into potential ammonia leakage scenarios that may arise during fuel transfer operations within confined spaces aboard marine vessels, such as the fuel preparation room and engine room. A high-fidelity three-dimensional model of the ammonia fuel preparation room was developed to simulate the dynamic dispersion behavior of leaked ammonia under various leak orientations. By analyzing the effects of five distinct leakage directions, the study reveals how the interaction between leak orientation, room geometry, ventilation layout, and thermal conditions significantly influences the spread and concentration of ammonia vapor. These findings provide critical insights for enhancing onboard safety systems, particularly in the strategic placement of gas sensors, the configuration of emergency ventilation systems, and the development of effective hazard mitigation protocols. Ultimately, this research supports the advancement of safer ammonia-fueled propulsion systems by minimizing toxic exposure and explosion risks in enclosed marine environments.

Ammonia explosions in confined spaces such as FPR pose significant risks due to the rapid propagation of overpressure waves. In this study, four key overpressure thresholds 20 kPa, 30 kPa, 50 kPa, and 100 kPa were used to categorize the severity of structural damage and human injury. These thresholds range from slight building damage and minor injuries to major structural failure and life-threatening conditions, enabling a detailed assessment of risk zones over time.

Simulation results showed that within the first 1.675 s after a leak and subsequent ignition, areas experiencing critical consequences such as fatal injuries or severe structural damage remained largely confined within a 10 m radius of the explosion source. However, zones exposed to lower overpressures ($\geq$20 kPa and $\geq$30 kPa) expanded significantly, with

the slight damage zone reaching up to 14.51 m. The minor injury zone encompassed the entire FPR, indicating a broader exposure risk for personnel compared to the concentrated area of critical hazards.

These spatial trends highlight a clear disparity between human vulnerability zones and structural impact areas. While fatal injury zones are relatively localized, structural damage zones are more widespread, underscoring the need for protective measures in building design. In particular, regions with dense piping infrastructure should adopt blast-resistant construction materials to reduce susceptibility to pressure-induced failures across multiple thresholds.

In conclusion, safety protocols must focus on rapid personnel evacuation from high-pressure impact zones and reinforce critical structures against overpressure. The findings also support the integration of risk-based zoning and emergency planning to account for the expanding influence of low to moderate overpressure effects. This comprehensive approach will enhance resilience in ammonia-fueled ship environments and other confined marine systems prone to gas explosion scenarios. Physical obstructions play a critical role in shaping both the behavior of ammonia dispersion and the resulting explosion dynamics. During gas release, the presence of vertical structures promotes upward migration and localized accumulation of ammonia, while simultaneously suppressing the lateral spread of the vapor cloud. When an explosion occurs, the surfaces of obstructions directly exposed to the blast are subjected to significantly intensified overpressure loads.

While this study provides a detailed numerical analysis of ammonia dispersion and explosion behavior within a confined marine fuel preparation room, certain limitations should be acknowledged. The use of a simplified global reaction mechanism for explosion modeling may not fully capture the complex chemical kinetics of ammonia combustion, including intermediate species and NO_x formation. Assumptions of uniform stoichiometric mixtures and ideal ignition conditions may deviate from real-world scenarios involving spatial heterogeneity and delayed ignition. The structural model excluded smaller obstructions that could significantly affect dispersion and flame propagation. Additionally, the empirical TNO Multi-Energy method, while practical, may produce conservative or imprecise results in highly obstructed environments. Future research should integrate detailed reaction mechanisms, transient thermal effects, and experimental validation to improve model accuracy and support safer ammonia-based marine fuel systems.

Abbreviations

The following abbreviations are used in this manuscript:

GHG	Greenhouse gas
IMO	The International Maritime Organization
SEEMP	The Ship Energy Efficiency Management Plan
EEDI	The Energy Efficiency Design Index
EEOI	The Energy Efficiency Operational Indicator
ICEs	Internal combustion engines
PFP	Power-to-fuel-to-power
FGSS	Fuel gas supply system
ER	Equivalence ratios
AF	Ammonia fractions
AFPV	Average flame propagation velocity
MEP	Maximum explosion pressure
LBV	Laminar burning velocity
VCE	Vapor cloud explosion
ME	TNO Multi-Energy
CFD	Computational Fluid Dynamics
STP	Standard temperature and pressure
PPE	Personal protective equipment
SCBA	Self-contained breathing apparatus
BLEVE	Boiling Liquid Expanding Vapor Explosion
FPR	Fuel preparation room
LNG	Liquefied natural gas
ME	Multi-Energy method
MP	Monitoring points
LEL	Lower explosive limit

References

1. Ni, P.; Wang, X.; Li, H. A review on regulations, current status, effects and reduction strategies of emissions for marine diesel engines. *Fuel* **2020**, *279*, 118477. [CrossRef]
2. Sèbe, M.; Scemama, P.; Choquet, A.; Jung, J.-L.; Chircop, A.; Razouk, P.M.-A.; Michel, S.; Stiger-Pouvreau, V.; Recuero-Virto, L. Maritime transportation: Let's slow down a bit. *Sci. Total. Environ.* **2022**, *811*, 152262. [CrossRef] [PubMed]
3. Li, R.; Liu, Y.; Wang, Q. Emissions in maritime transport: A decomposition analysis from the perspective of production-based and consumption-based emissions. *Mar. Policy* **2022**, *143*, 105125. [CrossRef]
4. Lee, H.; Ryu, B.; Anh, D.P.; Roh, G.; Lee, S.; Kang, H. Thermodynamic analysis and assessment of novel ORC- DEC integrated PEMFC system for liquid hydrogen fueled ship application. *Int. J. Hydrogen Energy* **2023**, *48*, 3135–3153. [CrossRef]
5. Duong, P.A.; Ryu, B.; Jung, J.; Kang, H. Thermal Evaluation of a Novel Integrated System Based on Solid Oxide Fuel Cells and Combined Heat and Power Production Using Ammonia as Fuel. *Appl. Sci.* **2022**, *12*, 6287. [CrossRef]
6. Duong, P.A.; Ryu, B.; Kim, C.; Lee, J.; Kang, H. Energy and Exergy Analysis of an Ammonia Fuel Cell Integrated System for Marine Vessels. *Energies* **2022**, *15*, 3331. [CrossRef]
7. The International Maritime Organization. *Resolution MEPC.305(73), Amendments to MARPOL Annex VI*; IMO: London, UK, 2018; Volume 1, pp. 1–15.
8. Zincir, B. Environmental and economic evaluation of ammonia as a fuel for short-sea shipping: A case study. *Int. J. Hydrogen Energy* **2022**, *47*, 18148–18168. [CrossRef]
9. Moon, K.; Wright, L.; Choi, S. DeRisk beta: Comparative Quantitative Risk Assessment (QRA) of fuel oil, LNG, methanol, and ammonia on a 15,000 TEU containership 2. Safety Risk of Conventional Containerships. *J. Adv. Mar. Eng. Technol.* **2025**, *49*, 42–46. [CrossRef]
10. Duong, P.A.; Ryu, B.R.; Jung, J.; Kang, H. A Comprehensive Review of the Establishment of Safety Zones and Quantitative Risk Analysis during Ship-to-Ship LNG Bunkering. *Energies* **2024**, *17*, 512. [CrossRef]
11. Duong, P.A.; Ryu, B.R.; Kyu, S.S.; Jeon, H.; Kang, H. Performance analysis of a fuel cells integrated system utilizing Liquified Natural Gas as fuel for a green shipping target. *Int. J. Nav. Arch. Ocean Eng.* **2023**, *15*, 100543. [CrossRef]

12. Duong, P.A.; Ryu, B.R.; Song, M.K.; Nam, D.; Kang, H. Thermodynamics analysis of a novel designation of LNG solid oxide fuel cells combined system with CO_2 capture using LNG cold energy. *J. Eng. Res.* **2023**, *12*, 226–238. [CrossRef]

13. Ye, M.; Sharp, P.; Brandon, N.; Kucernak, A. System-level comparison of ammonia, compressed and liquid hydrogen as fuels for polymer electrolyte fuel cell powered shipping. *Int. J. Hydrogen Energy* **2022**, *47*, 8565–8584. [CrossRef]

14. Ryu, B.; Duong, P.A.; Kang, H. Comparative analysis of the thermodynamic performances of solid oxide fuel cell–gas turbine integrated systems for marine vessels using ammonia and hydrogen as fuels. *Int. J. Nav. Arch. Ocean Eng.* **2023**, *15*, 100524. [CrossRef]

15. Jeong, S.; Kim, Y.; Kim, J.-S. Simulation and analysis of a fuel supply system with vent control system for ammonia fueled ships. *J. Adv. Mar. Eng. Technol.* **2024**, *48*, 260–267. [CrossRef]

16. Zhang, Y.H.P.; Mielenz, J.R. Renewable hydrogen carrier—Carbohydrate: Constructing the carbon-neutral carbohydrate economy. *Energies* **2011**, *4*, 254–275. [CrossRef]

17. Lamb, K.E.; Dolan, M.D.; Kennedy, D.F. Ammonia for hydrogen storage; A review of catalytic ammonia decomposition and hydrogen separation and purification. *Int. J. Hydrogen Energy* **2019**, *44*, 3580–3593. [CrossRef]

18. Herbinet, O.; Bartocci, P.; Dana, A.G. On the use of ammonia as a fuel—A perspective. *Fuel Commun.* **2022**, *11*, 100064. [CrossRef]

19. Yüzbaşıoğlu, A.E.; Avşar, C.; Gezerman, A.O. The current situation in the use of ammonia as a sustainable energy source and its industrial potential. *Curr. Res. Green Sustain. Chem.* **2022**, *5*, 100307. [CrossRef]

20. Yang, M.; Lam, J.S.L. Operational and economic evaluation of ammonia bunkering—Bunkering supply chain perspective. *Transp. Res. Part D Transp. Environ.* **2023**, *117*, 103666. [CrossRef]

21. Roy, A.; Srivastava, P.; Sinha, S. Dynamic failure assessment of an ammonia storage unit: A case study. *Process. Saf. Environ. Prot.* **2015**, *94*, 385–401. [CrossRef]

22. Kukkonen, J.; Savolainen, A.L.; Valkama, I.; Juntto, S.; Vesala, T. Long-range transport of ammonia released in a major chemical accident at Ionava, Lithuania. *J. Hazard. Mater.* **1993**, *35*, 1–16. [CrossRef]

23. Gaskin, S.; Pisaniello, D.; Edwards, J.W.; Bromwich, D.; Reed, S.; Logan, M.; Baxter, C. Application of skin contamination studies of ammonia gas for management of hazardous material incidents. *J. Hazard. Mater.* **2013**, *252–253*, 338–346. [CrossRef] [PubMed]

24. Anjana, N.; Amarnath, A.; Nair, M.H. Toxic hazards of ammonia release and population vulnerability assessment using geographical information system. *J. Environ. Manag.* **2018**, *210*, 201–209. [CrossRef] [PubMed]

25. Moura, R.; Beer, M.; Patelli, E.; Lewis, J.; Knoll, F. Learning from major accidents to improve system design. *Saf. Sci.* **2016**, *84*, 37–45. [CrossRef]

26. Michaels, R.A. Emergency Planning and the Acute Toxic Potency of Inhaled Ammonia. *Environ. Health Perspect.* **1999**, *107*, 617. [CrossRef]

27. Eliopoulou, E.; Papanikolaou, A.; Voulgarellis, M. Statistical analysis of ship accidents and review of safety level. *Saf. Sci.* **2016**, *85*, 282–292. [CrossRef]

28. Duong, P.A.; Ryu, B.R.; Jung, J.; Kang, H. Comparative analysis on vapor cloud dispersion between LNG/liquid NH3 leakage on the ship to ship bunkering for establishing safety zones. *J. Loss Prev. Process Ind.* **2022**, *85*, 105167. [CrossRef]

29. Zhang, Z.; Zhang, Z.; Zhou, Y.; Ouyang, Y.; Sun, J.; Zhang, J.; Li, B.; Zhang, D.; Wang, Y.; Yao, J.; et al. Review of the Diffusion Process, Explosion Mechanism, and Detection Technology of Hydrogen and Ammonia. *Energies* **2025**, *18*, 2526. [CrossRef]

30. Li, Y.; Bi, M.; Zhou, Y.; Zhang, Z.; Zhang, K.; Zhang, C.; Gao, W. Characteristics of hydrogen-ammonia-air cloud explosion. *Process Saf. Environ. Prot.* **2021**, *148*, 1207–1216. [CrossRef]

31. Li, S.; Chen, R.; Zhang, Y.; Cheng, S.; Li, X.; Zhang, T.; Zhang, X.; Zhou, W.; Shi, X.; Cao, W. The effect of NH3 concentration on explosion venting characteristics and combustion mechanism. *Int. J. Hydrogen Energy* **2024**, *101*, 1172–1182. [CrossRef]

32. Bae, J.; Noh, B.-S.; Lee, J.-W.; Choe, S.-J.; Park, K.-H.; Kim, J.-D.; Choi, J.-H. Quantitative Analysis of Explosion Characteristics Based on Ignition Location in an Ammonia Fuel Preparation Room Using CFD Simulation. *Appl. Sci.* **2025**, *15*, 6554. [CrossRef]

33. Tan, W.; Du, H.; Liu, L.; Su, T.; Liu, X. Experimental and numerical study of ammonia leakage and dispersion in a food factory. *J. Loss Prev. Process Ind.* **2017**, *47*, 129–139. [CrossRef]

34. Tan, W.; Lv, D.; Guo, X.; Du, H.; Liu, L.; Wang, Y. Accident consequence calculation of ammonia dispersion in factory area. *J. Loss Prev. Process Ind.* **2020**, *67*, 104271. [CrossRef]

35. Bouet, R.; Duplantier, S.; Salvi, O. Ammonia large scale atmospheric dispersion experiments in industrial configurations. *J. Loss Prev. Process Ind.* **2005**, *18*, 512–519. [CrossRef]

36. Murakami, T.; Kitabatake, N.; Tani, F. Dispersion in the Presence of Acetic Acid or Ammonia Confers Gliadin-Like Characteristics to the Glutenin in Wheat Gluten. *J. Food Sci.* **2015**, *80*, C269–C278. [CrossRef]

37. Al-Enazi, A.; Okonkwo, E.C.; Bicer, Y.; Al-Ansari, T. A review of cleaner alternative fuels for maritime transportation. *Energy Rep.* **2021**, *7*, 1962–1985. [CrossRef]

38. Ayvali, T.; Tsang, S.C.E.; Van Vrijaldenhoven, T. The position of ammonia in decarbonising maritime industry: An overview and perspectives: Part I. *Johns. Matthey Technol. Rev.* **2021**, *65*, 275–290. [CrossRef]

39. Yapicioglu, A.; Dincer, I. A review on clean ammonia as a potential fuel for power generators. *Renew. Sustain. Energy Rev.* **2019**, *103*, 96–108. [CrossRef]

40. Klerke, A.; Christensen, C.H.; Nørskov, J.K.; Vegge, T. Ammonia for hydrogen storage: Challenges and opportunities. *J. Mater. Chem.* **2008**, *18*, 2304–2310. [CrossRef]

41. Bicer, Y.; Dincer, I.; Zamfirescu, C.; Vezina, G.; Raso, F. Comparative life cycle assessment of various ammonia production methods. *J. Clean. Prod.* **2016**, *135*, 1379–1395. [CrossRef]

42. Le Fevre, C. *A Review of Demand Prospects for LNG as a Marine Transport Fuel*; Oxford Institute for Energy Studies: Oxford, UK, 2018.

43. Inal, O.B.; Dere, C.; Deniz, C. Onboard Hydrogen Storage for Ships: An Overview. In Proceedings of the 5th International Hydrogen Technologies Congress (IHTEC-2021), Online, 26–28 May 2021.

44. NCBI. Available online: https://pubchem.ncbi.nlm.nih.gov/compound/Ammonia (accessed on 1 June 2025).

45. McKinlay, C.J.; Turnock, S.; Hudson, D. A Comparison of hydrogen and ammonia for future long distance shipping fuels. In *LNG/LPG and Alternative Fuel Ships*; Royal Institute of Naval Architects: London, UK, 2020; pp. 53–65.

46. Stephens, H.W. The Texas City Disaster: A re-examination. *Ind. Environ. Crisis Q.* **1993**, *7*, 189–204. [CrossRef]

47. Babrauskas, V. Explosions of ammonium nitrate fertilizer in storage or transportation are preventable accidents. *J. Hazard. Mater.* **2016**, *304*, 134–149. [CrossRef] [PubMed]

48. Stewart, E. *Revisiting the Jonava Ammonia Tank Rupture—35 Years on*; Institution of Chemical Engineers: Rugby, UK, 2024; pp. 2–6.

49. Wasewar, K.L.; Kumar, M.S. Quantitative Risk Assessment. *i-Manag. J. Future Eng. Technol.* **2010**, *6*, 33–39. [CrossRef]

50. Zhang, T.X.; Li, M.R.; Liu, C.; Wang, S.P.; Yan, Z.-G. A review of the toxic effects of ammonia on invertebrates in aquatic environments. *Environ. Pollut.* **2023**, *336*, 122374. [CrossRef]

51. Fritt-Rasmussen, J.; Gustavson, K.; Aastrup, G.; Agersted, M.D.; Boertmann, D.; Clausen, D.S.; Jørgensen, C.J.; Lanso, A.S.; Mosbech, A. *Assessment of the Potential Environmental Impacts of a Major Ammonia Spill from a Power-to-X Plant and from Shipping of Ammonia in Greenland*; Aarhus University: Aarhus, Denmark, 2022.

52. Lin, W.; Luo, H.; Wu, J.; Hung, T.-C.; Cao, B.; Liu, X.; Yang, J.; Yang, P. A Review of the Emerging Risks of Acute Ammonia Nitrogen Toxicity to Aquatic Decapod Crustaceans. *Water* **2023**, *15*, 27. [CrossRef]

53. Zhu, G.; Guo, X.; Yi, Y.; Tan, W.; Ji, C. Experiment and simulation research of evolution process for LNG leakage and diffusion. *J. Loss Prev. Process Ind.* **2020**, *64*, 104041. [CrossRef]

54. Zhu, D.Z. Example of simulating analysis on LNG leakage and dispersion. *Procedia Eng.* **2014**, *71*, 220–229. [CrossRef]

55. Tofalos, C.; Jeong, B.; Jang, H. Safety comparison analysis between LNG/LH$_2$ for bunkering operation. *J. Int. Marit. Saf. Environ. Aff. Shipp.* **2020**, *4*, 135–150. [CrossRef]

56. Liu, Y.; Harikrishnan, B.; Kolluru, R.; Mastorakos, E. Computational fluid dynamics simulation of ammonia leakage scenarios during ship-to-ship bunkering. *Ocean Eng.* **2024**, *312*, 119136. [CrossRef]